the FEBS Journal

New insights into structure–function relationships of oxalyl CoA decarboxylase from *Escherichia coli*

Tobias Werther[1,*], Agnes Zimmer[1,†], Georg Wille[2], Ralph Golbik[1], Manfred S. Weiss[3] and Stephan König[1]

1 Department of Enzymology, Institute of Biochemistry & Biotechnology, Faculty for Biological Sciences, Martin Luther University Halle-Wittenberg, Halle, Germany
2 Institute of Biophysics, Johann Wolfgang Goethe University Frankfurt am Main, Germany
3 Macromolecular Crystallography (BESSY-MX), Electron Storage Ring BESSY II, Helmholtz Zentrum Berlin für Materialien und Energie, Albert Einstein Straße 15, Berlin, Germany

Keywords
ADP activation; crystal structure; oxalate degradation; thiamine diphosphate; X-ray scattering

Correspondence
S. König, Institute of Biochemistry & Biotechnology, Martin Luther University Halle-Wittenberg, Kurt Mothes Straße 3, 06120 Halle (Saale), Germany
Fax: +49 345 5527014
Tel: +49 345 5524829
E-mail: stephan.koenig@biochemtech.uni-halle.de
Website: http://www.biochemtech.uni-halle.de/enzymologie/

Present address
*Humboldt University Berlin, Institute of Biology, Research Group Structural Biology & Biochemistry, Germany
†Research Group Macromolecular Interactions, Division of Structural Biology, Helmholtz Centre for Infections Research, Braunschweig, Germany

Database
Structural data for holo-*Ec*ODC (ThDP-*Ec*ODC) in the absence of additional ligands and in complex with either ADP or acetyl CoA have been submitted to the Protein Data Bank under the accession numbers 2q27, 2q28 and 2q29, respectively.

(Received 28 January 2010, revised 26 March 2010, accepted 8 April 2010)

doi:10.1111/j.1742-4658.2010.07673.x

The gene *yfdU* from *Escherichia coli* encodes a putative oxalyl coenzyme A decarboxylase, a thiamine diphosphate-dependent enzyme that is potentially involved in the degradation of oxalate. The enzyme has been purified to homogeneity. The kinetic constants for conversion of the substrate oxalyl coenzyme A by the enzyme in the absence and presence of the inhibitor coenzyme A, as well as in the absence and presence of the activator adenosine 5′-diphosphate, were determined using a novel continuous optical assay. The effects of these ligands on the solution and crystal structure of the enzyme were studied using small-angle X-ray scattering and X-ray crystal diffraction. Analyses of the obtained crystal structures of the enzyme in complex with the cofactor thiamine diphosphate, the activator adenosine 5′-diphosphate and the inhibitor acetyl coenzyme A, as well as the corresponding solution scattering patterns, allow comparison of the oligomer structures of the enzyme complexes under various experimental conditions, and provide insights into the architecture of substrate and effector binding sites.

Structured digital abstract

- MINT-7717846: *EcODC* (uniprotkb:P0AFI0) and *EcODC* (uniprotkb:P0AFI0) *bind* (MI:0407) by *X-ray scattering* (MI:0826)
- MINT-7717834: *EcODC* (uniprotkb:P0AFI0) and *EcODC* (uniprotkb:P0AFI0) *bind* (MI:0407) by *X-ray crystallography* (MI:0114)

Abbreviations
*Ec*ODC, oxalyl CoA decarboxylase from *Escherichia coli*; *Of*ODC, oxalyl CoA decarboxylase from *Oxalobacter formigenes*; PADP, 3′-phosphoadenosine 5′-diphosphate; ThDP, thiamine diphosphate.

Introduction

Oxalic acid is toxic for many organisms. However, some bacteria (e.g. *Oxalobacter formigenes*) are able to tolerate oxalate and even use it as an exclusive energy source [1]. Oxalyl CoA represents an activated form of oxalate and is decarboxylated by the thiamine diphosphate (ThDP)-dependent enzyme oxalyl CoA decarboxylase (ODC, EC 4.1.1.8) [2]. Baetz & Allison [2] published the first biochemical analysis of *Of*ODC, indicating that it is a homotetramer in solution. Recently, Berthold *et al.* [3,4] determined the crystal structure and postulated a catalytic mechanism on the basis of this structure. The monomer has three domains and its topology is typical of ThDP enzymes [5]. Interestingly, in addition to the cofactors ThDP and Mg^{2+}, one molecule of ADP was bound per monomer distant from the CoA binding site. Furthermore, kinetic experiments revealed that ADP significantly activates *Of*ODC, whereas ATP was only a weak activator [3]. Although the mechanism of activation by ADP remains to be elucidated, the authors postulated its physiological relevance. To date, more than 50 oxalotrophic bacteria that are capable of using oxalate as a carbon and energy source have been identified [6]. The Swiss-Prot/TREMBL database includes 28 highly homologous sequence entries encoding putative ODCs. Only a few of these have been isolated and characterized, such as those from *Oxalobacter formigenes* [2–4] and *Pseudomonas oxalaticus* [7]. Figure 1 shows the high degree of similarity of the deduced amino acid sequences of the enzymes from *Escherichia coli* and *O. formigenes*. Although no oxalotrophic metabolism has yet been reported for *E. coli*, its genome contains open reading frames that encode a putative formyl CoA transferase (*yfdW*) and an ODC

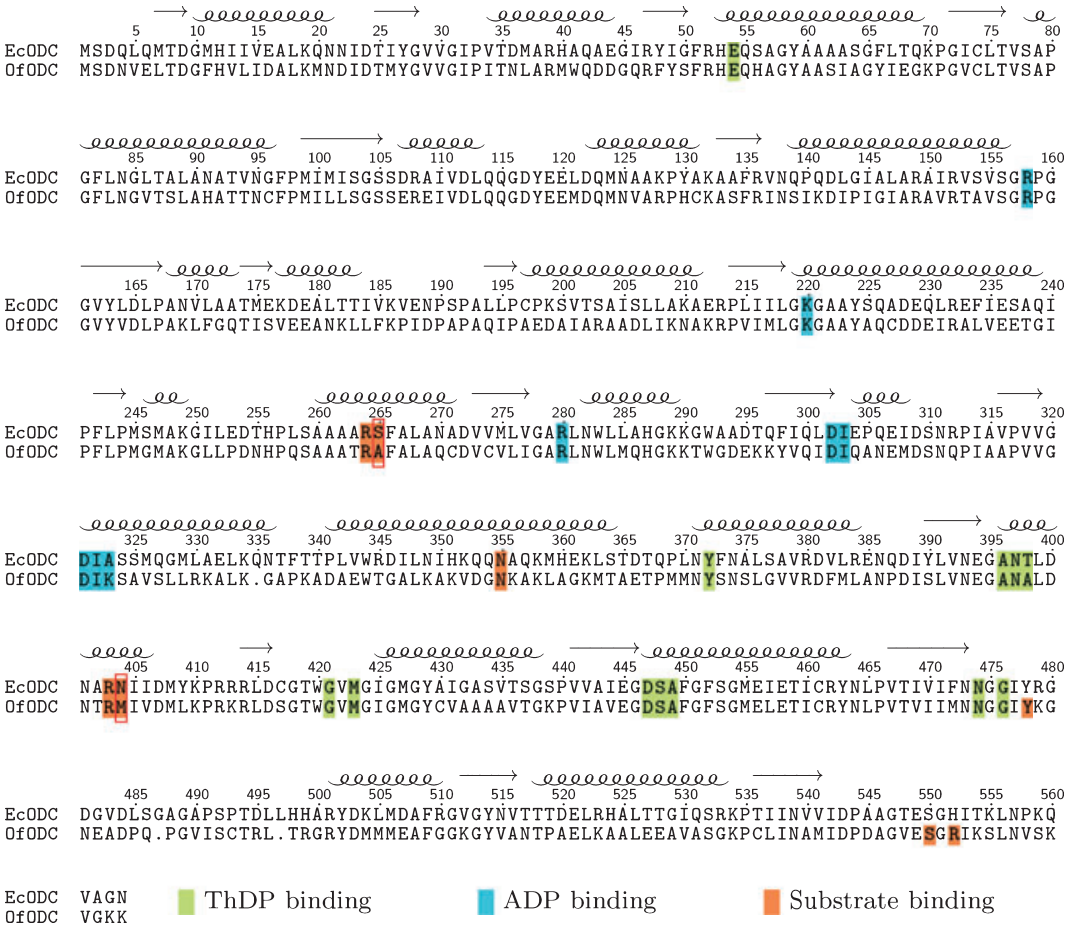

Fig. 1. Sequence alignment of *Ec*ODC and *Of*ODC. Secondary structure elements are included (arrows, β sheets, spirals, α helices). Ligand binding sites are indicated in green for the cofactor ThDP, in blue for the activator ADP, and in orange for the substrate (here PADP). Different amino acid residues at the substrate binding site are indicated by red boxes.

(*yfdU*, 564 amino acids, 60.581 Da). Thus, it was interesting to clarify whether these enzymes do indeed fulfil their predicted function, and how the properties of the enzymes differ from those of the homologous enzymes from *O. formigenes*. Although the crystal structure and kinetic properties of formyl CoA transferase from *E. coli* were recently determined [8,9], knowledge on *Ec*ODC is lacking.

Here, we present the first results of functional and structural studies on purified *Ec*ODC in the presence of activators and inhibitors using various methods, such as steady-state kinetic measurements, small-angle X-ray solution scattering (SAXS) and protein crystal structure analysis.

Results

Expression and purification

*Ec*ODC was expressed in *E. coli* strain BL21, and purified by homogenization, streptomycin sulfate and ammonium sulfate precipitation steps, dialysis, anion-exchange chromatography, and size-exclusion chromatography. Approximately 150 mg of homogeneous, ThDP-free apoenzyme was obtained from 1 L of cell culture.

Crystal structure of EcODC complexes

Overall structure

Holo-*Ec*ODC (ThDP-*Ec*ODC) was crystallized in the absence of additional ligands (PDB ID 2q27) and in complex with either ADP (2q28) or acetyl CoA (2q29). The ortho-rhombic crystals obtained all belong to space group $C222_1$ (Table 1). The enzyme tetramer is a dimer of dimers, and displays twofold symmetry. The interface area between the monomers of a functional dimer is significantly larger than the interface between dimers. For most of the polypeptide chains, the electron density is well defined, excluding residues 1–4 and 551–564 (555–564 for the ADP complex) in both chains. Residue Y478 at the active site assumes a rare conformation that falls in a disallowed region of the Ramachandran plot (data not shown). However, the electron density of the side chain of Y478 is well defined. The same is true for the corresponding residue Y483 in the crystal structure of *Of*ODC.

No significant differences were found between the overall structures of all three *Ec*ODC complexes (Fig. 2, rmsd 0.18 Å for 1043 superimposed Cα atom pairs of 2q27 and 2q28, rmsd 0.14 Å for 1023 superimposed Cα atom pairs of 2q27 and 2q29, and rmsd 0.16 Å for 993 superimposed Cα atom pairs of 2q28 and 2q29), indicating that binding of the activator ADP or the inhibitor acetyl CoA does not induce significant conformation changes within the dimers. However, four additional amino acid residues at the C-terminus were pinpointed in the presence of the activator ADP that are not defined in the absence of this ligand.

The *Ec*ODC monomer displays the typical binding fold of ThDP enzymes, comprising three domains of the α/β type, designated as the PYR domain (residues 1–190), the R domain (residues 191–368) and the PP domain (residues 369–564) [5] (Fig. 2A). The overall structure of the monomer is highly similar to that of *Of*ODC (rmsd 0.62 Å for 488 superimposed Cα atom pairs). The locations of the cofactor ThDP and the activator ADP are clearly defined in the electron density map. In contrast, electron density of the *S*-acetyl pantetheine moiety of the inhibitor acetyl CoA is not detectable. Thus, only the 3′-phosphoadenosine 5′-diphosphate (PADP) moiety of acetyl CoA was included in the model.

Active site

Two molecules of the cofactor ThDP are bound in the canonical V conformation at the interface between the PYR domain and the PP domain of two subunits of the functional dimer. The main chain oxygen of G421 and the side-chain carboxyl oxygen of E54 interact with the amino pyrimidine moiety of ThDP (Fig. 3); these are highly conserved interactions in ThDP enzymes [10]. The diphosphate moiety is stabilized by interactions with residues Y372, A396, N397 and T398 of the PP domain, as well as by interactions with the octahedrally coordinated magnesium ion. Based on the architecture of the active site, a functional role may only be suggested for residue E54. Its direct interaction with the N1′ nitrogen atom of ThDP enables cofactor activation (ylid formation). This kind of interaction is found in all crystal structures of ThDP enzymes except glyoxylate carboligase [11]. Some other moieties may be involved in catalysis, for instance the preserved water molecule interacting with residues I32, Y118 and E119 can act as a general base for deprotonation of intermediates, as proposed by Berthold *et al.* [3,4] for *Of*ODC. The tyrosine residues 118 and 478 (the latter in an uncommon side-chain conformation) stabilize the oxalyl moiety of the substrate as demonstrated for the corresponding *Of*ODC structure [4]. However, the electron density of the *S*-acetyl-pantetheine moiety of acetyl CoA was very poor in the corresponding ThDP–acetyl CoA–*Ec*ODC complex.

Table 1. Data collection and refinement statistics for three *Ec*ODC complexes (numbers in parentheses correspond to the highest-resolution shell).

	ThDP–*Ec*ODC	ThDP–ADP–*Ec*ODC	ThDP–acetyl CoA–*Ec*ODC
Data collection			
Beamline	X12	X12	BW7A
Wavelength (Å)	0.93001	0.93001	0.9785
Crystal–detector distance (mm)	220	175	130
Rotation range per image (degrees)	0.5	0.5	0.3
Total rotation range (degrees)	200	180	180
Space group	$C222_1$	$C222_1$	$C222_1$
Detector	MARCCD-225	MARCCD-225	MARCCD-165
Cell dimensions (Å)	132.11 × 145.44 × 147.98	132.27 × 143.62 × 147.58	132.57 × 145.53 × 147.19
Resolution (Å)	99.0–2.12 (2.16–2.12)	99.0–1.74 (1.77–1.74)	99.0–1.82 (1.85–1.82)
Number of observed reflections (unique)	565 267 (80 614)	1 023 314 (143 107)	915 365 (126 889)
R_{merge} (%)	10.7 (73.9)	10.4 (86.8)	5.2 (25.7)
I/σ (I)	16.8 (2.3)	18.8 (2.3)	35.5 (7.7)
Completeness (%)	99.8 (99.9)	99.9 (100)	99.9 (100)
Redundancy	7.0	7.2	7.2
Mosaicity (degrees)	1.19	0.65	0.49
B factor (Wilson plot, Å^2)	37	20	20
Refinement			
Resolution (Å)	18.3–2.12 (2.17–2.12)	20.6–1.74 (1.78–1.74)	42.3–1.82 (1.87–1.82)
Total number of atoms	8798	9344	9037
Number of atoms (protein)	8153	8280	8191
Number of atoms (water)	515	907	707
R_{free} (%)	23.7	19.6	19.4
R_{work} (%)	19.3	17.7	17.5
Average B factors (Å^2)			
Protein	36.55	19.17	19.07
ThDP	30.29	18.83	15.28
Ligand		14.79 (ADP)	24.51 (PADP)
Water	39.48	29.12	26.12
rmsd			
Bond lengths (Å)	0.023	0.012	0.014
Bond angles (°)	1.9	1.4	1.4
Ramachandran plot			
Favoured (%)	90.3	90.3	90.3
Allowed (%)	9.5	9.5	9.5
Disallowed	Y478	Y478	Y478
PDB deposit ID	2q27	2q28	2q29

ADP binding site

ADP binds to *Ec*ODC at a Rossmann fold in a cleft between the PYR domain and the PP domain. As for ThDP, ADP molecules are found in all four subunits of the tetramer, but, in contrast to ThDP, the binding domains are recruited from one subunit only. The main chain nitrogens of residues I322 and I303 interact with nitrogen atoms of the adenine ring and the γ-carboxyl group of the side chain of residue D302, the δ and ω nitrogen atoms of the guanodino group of R158 interact with the hydroxyl groups of ribose, and the main chain nitrogens of K220 and R280 interact with the 5′-diphosphate moiety (Fig. 4A). The side chains of I322 and I303 form a hydrophobic pocket surrounding the planar adenosine ring system. As mentioned above, the overall crystal structures of the *Ec*ODC complexes are almost identical. However, the mean B factor for the protein atoms of 2q27 (approximately 37 Å^2) is almost twice that of crystal structures with additional ligands (2q28 and 2q29, both approximately 19 Å^2, see Table 1). This freezing effect of the ligand ADP is particularly pronounced for the C-terminal part of the subunits. Hence, four additional residues are included in the model 2q28 compared to 2q27. Thus, binding of the activator ADP stabilizes the C-terminus. As in other ThDP enzymes, this part of the structure runs across the active site and may support catalysis by exclusion of solvent.

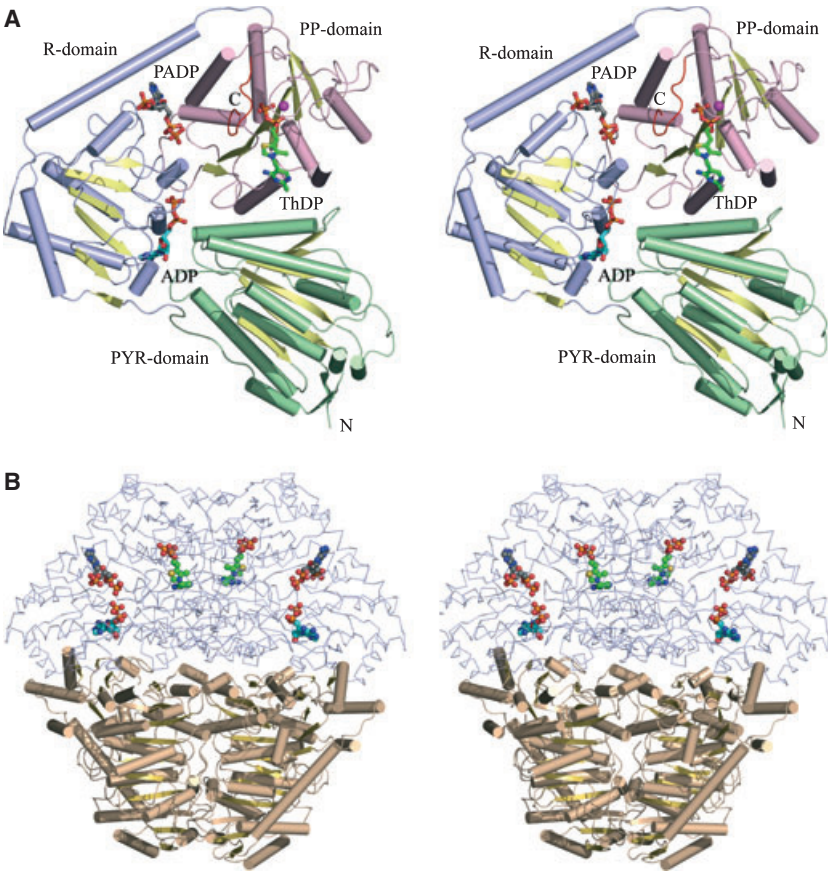

Fig. 2. Stereo view of the crystal structure of *Ec*ODC. (A) Schematic representation of the *Ec*ODC monomer. Yellow arrows indicate β sheets, and cylinders indicate helices (green, PYR domain; blue, R domain; pink, PP domain). To illustrate the binding sites for the substrate (PADP in this model), activator (ADP) and cofactor (ThDP), the image represents a superposition of three complexes, ThDP–*Ec*ODC (2q27), ThDP–ADP–*Ec*ODC (2q28) and ThDP–acetyl CoA–*Ec*ODC (2q29), and ligands are shown as sticks. The N- and C-termini are also indicated. (B) Views of the tetramer assembly of *Ec*ODC. Functional dimers are presented as traces of Cα atoms (grey lines) with ligands overlaid (ThDP, ADP and PADP, shown as spheres), and as schematic secondary structures (α helices indicated as brown cylinders, β sheets indicated as yellow arrows).

Substrate binding site

Due to the wide-stretched chemical structure of the substrate oxalyl coenzyme A, the substrate binding pocket must be considerably larger than the actual active site. For the crystal structure of the ThDP–*Ec*ODC complex with the substrate analogue acetyl CoA, additional electron density was found in the cleft between the R domain and the PP domain of one subunit, which was assigned to the PADP moiety of the substrate analogous inhibitor acetyl CoA (Fig. 4B). Unfortunately, no continuous electron density was found for the *S*-acetyl pantetheine part of acetyl CoA, and consequently the model for the inhibitor remains incomplete. The nitrogen atom of the amino group of the adenosine ring of PADP interacts with residue N404. The oxygen of the α phosphate of ribose diphosphate is stabilized by interactions with the ω nitrogen of the guanidino group of residue R403 and the γ carbonyl oxygen of residue N404. The 3′-phosphate is stabilized by interaction of two of its oxygens with the side-chain oxygen and nitrogen of residues S265 and N355, respectively. The PADP moiety in the structure of the ThDP–acetyl CoA–*Ec*ODC complex

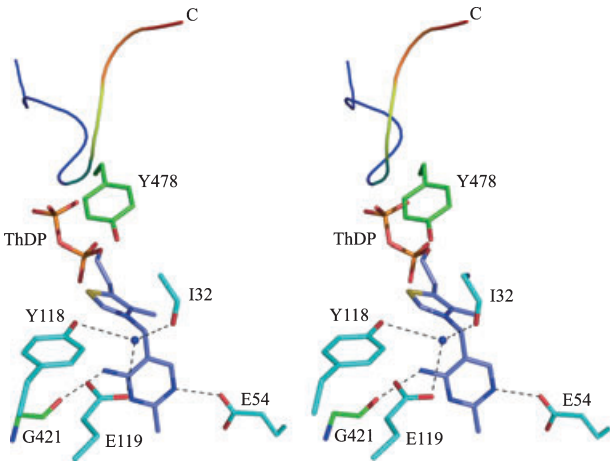

Fig. 3. Stereo view of the active site of *Ec*ODC. Only amino acid residues (different colours indicating different subunits) and a water molecule (blue sphere) adjacent to the thiamine moiety of the cofactor are shown. Black dashed lines indicate hydrogen bonds. The C-terminal region is coloured according to the observed B factors (blue, low; red, high).

superimposes neatly with the corresponding parts of oxalyl CoA in the *Of*ODC structure [4]. Differences are observable only in the number of hydrogen bonds

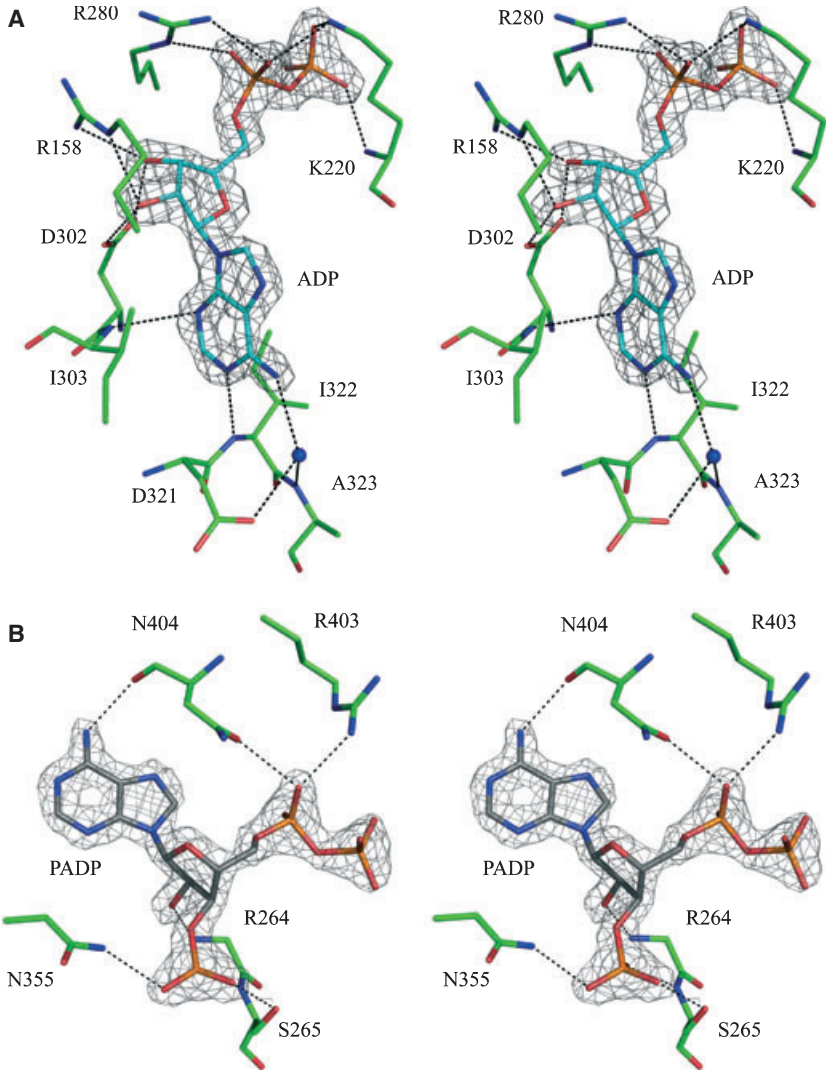

Fig. 4. Stereo views of the binding sites of *Ec*ODC for ADP (A) and PADP (B). The $2F_0 - F_c$ electron density of the ligands is contoured at 2.5 σ. Hydrogen bonds are shown as black dashed lines, and the water molecule is shown as a blue sphere.

(Fig. 4B). Two additional interactions occur in *Ec*ODC between PADP and residues S265 and N404, respectively.

Small-angle X-ray solution scattering

SAXS studies were performed to characterize the influence of various effectors on the solution structure of the enzyme, and to compare the three crystal structure complexes with the corresponding complexes in solution. Thus conditions close to those for crystallization were used for SAXS measurements (for details, see Experimental procedures). Information on the quaternary structure of the catalytically competent *Ec*ODC species in solution was obtained from the enzyme concentration dependence of scattering of the ThDP–*Ec*ODC complex (0.9–22 mg·mL^{-1}, Fig. 5A). By extrapolating the resulting dependence of the scattering parameters R_G and $I_{(0)}$ to infinite dilution, a R_G value of approximately 3.9 nm was obtained, which is a typical value for the tetrameric state of ThDP-dependent enzymes. The same is true for the molecular mass calculated from $I_{(0)}$ of *Ec*ODC using BSA as a molecular mass standard. Given the calculated monomer masses of 60.6 kDa, the empirically obtained value of 230 kDa represents a tetramer. The decrease of scattering parameters at high enzyme concentration is indicative of repulsive interactions between macromolecules [12,13]. This behaviour was independent of the ligand present (ThDP, ADP or CoA) and was also found for other ThDP-dependent enzymes [14,15].

As shown in the crystal structures of *Ec*ODC complexes presented here the cofactors are bound non-covalently in the interface between two subunits of one dimer. Two dimers with four bound ThDP molecules form the catalytically active tetrameric structure

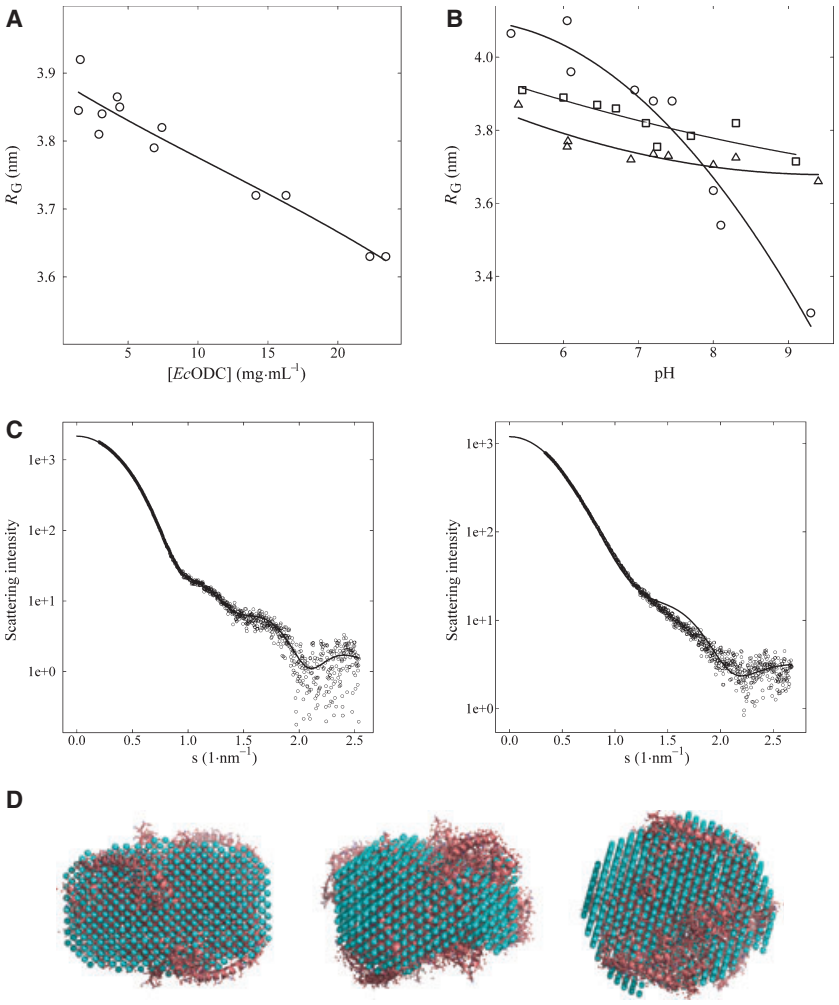

Fig. 5. Small-angle X-ray solution scattering of *Ec*ODC. (A) Dependence of the scattering parameter R_G on the concentration of *Ec*ODC in the presence of 10 mM ThDP/$MgSO_4$ (open circles). The line is shown for better visualization only. (B) pH dependence of the scattering parameter R_G of apo-*Ec*ODC (open circles), apo-*Ec*ODC in the presence of 10 mM ThDP/$MgSO_4$ (triangles), and apo-*Ec*ODC in the presence of 10 mM ADP (squares), respectively. Lines are shown for better visualization only. (C) Superposition of experimental scattering patterns of *Ec*ODC solutions (open grey circles) and theoretical patterns calculated from the crystal structure model 2q27 (black solid lines). Left, 2.9 mg *Ec*ODC·mL^{-1}, 10 mM ThDP, pH 6.9 (χ = 1.195); right, 4.6 mg EcODC·mL^{-1} (apo-enzyme), pH 9.3 (χ = 3.032). (D) Superposition of structure models of the ADP-*Ec*ODC complex in crystal and solution. The crystal structure of 2q28 is shown in ribbon and line style in deepsalmon, the solution structure model of ADP-ThDP-*Ec*ODC calculated from experimental scattering patterns using the program DAMMIN [29] is shown as aquamarin spheres. The structures on the left hand side are rotated 90° around the y axis (middle) and z axis (right hand side).

(Fig. 2B). In the case of ThDP enzymes, the oligomeric state does not only depend on enzyme concentration [14], but also on the pH value. Figure 5B illustrates the influence of pH on the oligomer structure of *Ec*ODC. In the optimum range of catalytic activity, pH 5.5–7.0, the scattering parameters indicate a tetrameric state of the enzyme (R_G 3.9–4 nm, molecular mass 200–220 kDa). However, above pH 7.5, the R_G values start to decrease, indicating oligomer dissociation. The value of 3.3 nm at pH 9.3 corresponds to the monomeric state (Fig. 2A). The presence of the cofactor ThDP or the activator ADP cannot completely prevent oligomer dissociation, but stabilizes the tetrameric state against increasing pH. Even at pH 9.1, R_G values of 3.7 nm and molecular masses of 150–160 kDa were obtained for ThDP–*Ec*ODC and ADP–*Ec*ODC solutions. These values are typical for dimers.

As stated above, the crystal structures of the three complexes do not differ significantly in their overall structure. In order to determine whether the same is true for the structure of the complexes in aqueous solutions, crystal and solution structures were compared. Superposition of structures can be performed on the basis of 3D models or using experimental SAXS data and scattering patterns calculated from crystal structure models. In the first case, structure models are calculated *ab initio* from SAXS scattering patterns (Fig. 5D). However, the resulting solution structure models are not unique because of extrapolation from 1D experimental data to 3D models with low spatial resolution (maximum 2.5 nm). Therefore, we prefer data comparison in reciprocal space. Using the program CRYSOL [16] from the ATSAS program suite for small-angle scattering data analysis from biological macromolecules, theoretical scattering patterns can be calculated from the crystal structure models and overlaid on experimental scattering patterns. The degree of similarity can be evaluated from the resulting χ values [16]. The best fits to crystal structures were obtained for ADP–*Ec*ODC and ThDP–

*Ec*ODC solutions at 3 mg *Ec*ODC·mL^{-1} and pH 6.9 (Fig. 5C). When the corresponding scattering patterns were superimposed on the calculated patterns of the three crystal structure models 2q27, 2q28 and 2q29, no significant differences were obtained at a spatial resolution of 2.5 nm (χ values of 1.192, 1.492, 1.264 and 1.195, 1.377, 1.382, respectively). The high degree of accordance is also obvious from superposition of the solution and crystal structure models (Fig. 5D).

Using dimers and tetramers of the crystal structure model 2q27, the best fits for apoenzyme solutions at various pH values were obtained for the dimer at pH 9.3 (χ 3.032, Fig. 5C) and for the tetramer at pH 6.95 (χ 3.881), respectively. On one hand, this confirms the conclusion from the SAXS studies on the pH dependence of oligomer dissociation. On the other hand, the higher χ values demonstrate conformational differences between the apoenzyme of *Ec*ODC in solution and the crystal structure of the ThDP–*Ec*ODC complex. These structural deviations are illustrated by significant differences between experimental and calculated scattering patterns at *s* values of 1–1.5 nm^{-1} (Fig. 5C).

Novel continuous kinetic assay

Previous kinetic studies on ODCs were performed either discontinuously by monitoring the decarboxylation of oxalyl CoA to formyl CoA by HPLC and capillary electrophoresis, respectively [17,18], or continuously by using two auxiliary enzymes, formate dehydrogenase and formyl CoA transferase [2]. Here, a kinetic assay was established to directly monitor changes in the UV absorbance of the substrate oxalyl CoA during catalysis. Oxalyl CoA was synthesized [19] and further purified by reverse-phase HPLC [20]. The novel assay is based on spectroscopic studies by Quayle [7] reporting that decarboxylation of oxalyl CoA is accompanied by a decrease in absorbance at 265 nm and a concomitant increase at 235 nm (Fig. 6A). An absorbance coefficient of 3300 M^{-1}·cm^{-1} at 235 nm and pH 6.5 was determined for the purified oxalyl CoA in the present study. All kinetic measurements were performed by directly monitoring the increase in absorbance at 235 nm, which corresponds to the decarboxylation of oxalyl CoA. The progress curves (Fig. 6B) illustrate that (a) a clear signal is detectable even at low substrate concentrations; (b) steady state is readily established as illustrated by the linearity in the early stage of the progress curves; (c) substrate is completely converted; and (d) the non-enzymatic reaction is not significant, as expected. Thus, the continuous assay provides quantitative information on formation of formyl CoA in a simple to perform manner.

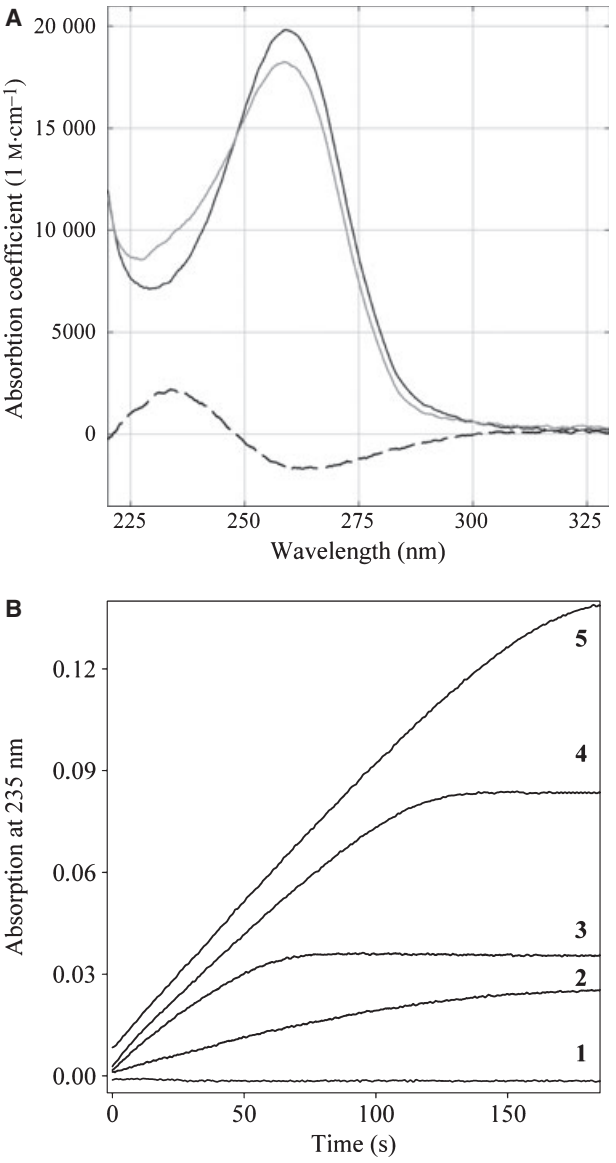

Fig. 6. Spectral changes during decarboxylation of oxalyl CoA. (A) UV/Vis spectra of oxalyl CoA (solid black line) and formyl CoA (solid dark grey line) dissolved in 25 mM sodium phosphate, pH 6.5. The dashed line indicates the difference spectrum. (B) Progress curves for the catalytic decarboxylation of oxalyl CoA (1, 0 μM; 2, 10 μM; 3, 16.0 μM; 4, 35 μM; 5, 50 μM) by *Ec*ODC (0.26 μg·mL^{-1}) at 30 °C.

Kinetic characterization

The steady-state kinetics displayed Michaelis–Menten behaviour under all conditions used. The pH optimum for the catalytic activity of *Ec*ODC was in the broad

pH range 5.5–7.0. Similar ranges have been reported for ODCs from *O. formigenes* and *P. oxalaticus* [2,7]. For the substrate oxalyl CoA, a K_M of 4.8 μM and a k_{cat} of 60.7 per second and subunit were determined from steady-state measurements at pH 6.5 and 30 °C (Fig. 7 and Table 2). *Ec*ODC has a considerably higher catalytic efficiency (k_{cat}/K_M) than *Of*ODC (12.6 versus 3.8 $mM^{-1}\cdot s^{-1}$). This is mainly due to the fivefold lower K_M of oxalyl CoA [3]. The SAXS studies imply that the tetrameric state is the catalytically active one. Coenzyme A competitively inhibits the decarboxylation catalysed by *Ec*ODC (K_I of 80 μM; Fig. 7A and Table 2). However, the affinity of CoA for *Ec*ODC is five times higher than that for *Of*ODC, for which weak mixed-type inhibition (400 and 270 μM) was found. In the case of *Ec*ODC, the presence of 300 μM ADP, an activator of ODC catalysis, resulted in a marginal increase in k_{cat} and a small decrease in K_M, leading to a 1.7-fold higher catalytic efficiency (Fig. 7B and Table 2). Similar weak activating effects have been observed for ATP and AMP (data not shown). An approximately threefold increase in catalytic activity was observed for *Of*ODC in the presence of ADP [3]. Obviously, the physiological importance of ADP activation as postulated for *O. formigenes* is weaker for *E. coli*, as oxalate degradation seems to play no role in energy generation in the latter organism under normal environmental conditions.

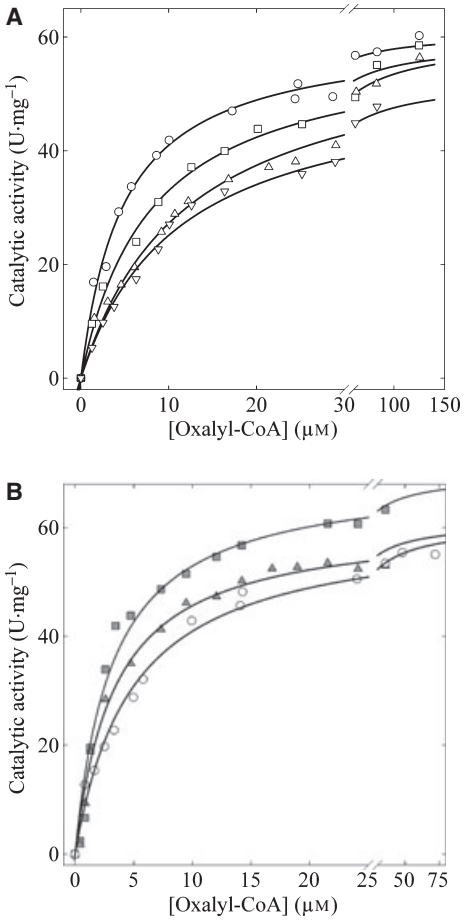

Fig. 7. Influence of the inhibitor CoA and the activator ADP on the steady-state kinetics of *Ec*ODC catalysis. (A) Plots of *v* against [S] in the absence (circles) and presence of various concentrations of CoA (squares, 30 μM; triangles, 60 μM; inverse triangles, 120 μM; lines, hyperbolic fits). (B) Plots of *v* against [S] in the absence (open circles) and presence of 60 μM (filled triangles) and 300 μM ADP (filled squares), respectively. Lines indicate hyperbolic fits. The concentration of *Ec*ODC was 0.26 $\mu g\cdot mL^{-1}$.

Table 2. Kinetic constants for the decarboxylation of oxalyl CoA catalysed by *Ec*ODC in the absence and presence of the inhibitor CoA and the activator ADP. The errors given are the fitting errors.

Additions	K_M (μM)	k_{cat} (s^{-1})	k_{cat}/K_M ($s^{-1}\cdot\mu M^{-1}$)
None	4.82 ± 0.31	60.7 ± 0.89	12.6
30 μM CoA	7.95 ± 0.68	59.2 ± 1.31	7.4
60 μM CoA	12.00 ± 0.71	59.9 ± 1.14	5.0
120 μM CoA	11.02 ± 0.73	52.8 ± 1.15	4.8
60 μM ADP	3.37 ± 0.35	61.1 ± 1.57	18.1
300 μM ADP	3.17 ± 0.45	69.7 ± 2.66	22.0

Discussion

Our results show that the gene *yfdU* from *E. coli* encodes an enzyme that exhibits oxalyl CoA decarboxylase activity *in vitro*. Three crystal structures of *Ec*ODC complexes (with the cofactor ThDP, with ThDP and the activator ADP, and with ThDP and the substrate analogue acetyl CoA, respectively) indicate a tetrameric enzyme, with binding of neither ThDP, ADP nor PADP (the part of acetyl CoA found in the crystal structure) inducing significant alterations of the protein conformation. This is also valid for the solution structures as determined using SAXS. Superposition of solution and crystal structures showed a very high degree of accordance, except for ThDP–acetyl CoA–*Ec*ODC. The scattering patterns of the latter do not match any of the crystal structures, indicating that binding of acetyl CoA may induce changes in the protein conformation in solution. Berthold *et al.* [4] published crystal structures of *Of*ODC in complex with the substrate, the post-decarboxylation intermediate and the product. The only difference between these structure complexes and that for holo-*Of*ODC without additional ligands [3] was a ligand induced ordering of the C-terminus (residues 553–565). For *Ec*ODC, the only structural effect of binding of ADP was a partially ordered C-terminus (residues 551–555). In

both enzyme species, the C-terminal part of the subunits is not involved in crystal packing contacts. From these results, it may be concluded that the prime effect of ADP activation on the enzyme conformation is the freezing of this part of the subunit to reduce its flexibility and thus to shield the active site from the environment. This is likely to enhance the rate of cofactor activation (deprotonation of the C2 atom of ThDP [21]) as well as the rate of decarboxylation [22]. A similar activation mechanism is probably operative in pyruvate decarboxylases from yeast species [21].

Although the crystal structures of the holoenzyme species from *E. coli* and *O. formigenes* are virtually identical, the enzymes differ in their kinetic behaviour. This difference is not obvious from the crystal structure of the ThDP binding sites formed by identical amino acid residues in both species. However, in the case of *Of*ODC, a thiazolon cofactor analogue was found at the active site even though ThDP was added to the crystallization mixture. The reason for this striking difference is as yet unclear. The significantly higher affinities of the substrate oxalyl CoA and the inhibitor CoA for *Ec*ODC may be caused by two additional hydrogen bond interactions (S265 and N404) in the substrate binding site found for PADP in this enzyme species. The corresponding side chains in *Of*ODC (A267 and M409) do not tend to form hydrogen bonds with either the substrate or the inhibitor. Thus, these structural differences could well be the reason for the kinetic differences seen between the two enzyme species. On the other hand, the differing kinetic constants could be also partially due to the different assays used, our novel continuous spectroscopic one for *Ec*ODC and the discontinuous HPLC-based assay for *Of*ODC. The continuous assay appears to be the more reliable and more direct approach, as whole progress curves can be conveniently recorded.

The identical architecture of the ADP binding sites of both species means that no structural explanation is possible for the differing activating effects of ADP. However, electron density for ADP was found in the crystal structure of *Of*ODC, even when no ligand was added [3]. ADP was clearly detectable in the structure of *Ec*ODC only if the ligand was present during crystallization. The poor ADP activation of *Ec*ODC presumably reflects the minor physiological relevance of oxalate degradation for the energy metabolism of *E. coli*. Thus, it is conceivable that non-oxalotrophic bacteria only require enzymes for oxalate detoxification under certain conditions [9]. Future studies of other putative oxalyl CoA decarboxylases are required to unravel this phenomenon, as well as the molecular basis of ADP activation.

Experimental procedures

Unless otherwise stated, all chemicals and reagents were purchased from Sigma-Aldrich Chemie GmbH (Steinheim, Germany), VWR International GmbH (Darmstadt, Germany) or AppliChem GmbH (Darmstadt, Germany), and were of the highest available purity.

Protein expression and purification

The plasmid pMS470-115/6/5 was generously supplied by Johannes Steinreiber (Dept. for Organic Chemistry, University of Graz, Austria). It carries the gene for oxalyl CoA decarboxylase from *E. coli* under the control of a Tac promoter, and was used to transform *E. coli* BL21 cells. The cells were grown at 30 °C in 2 × YT-ampicillin medium (1% w/v yeast extract, 2% w/v tryptone, 1% w/v NaCl and 50 $\mu g \cdot mL^{-1}$ ampicillin) in shaking flasks. When the solution had reached an absorbance of 0.8 at 600 nm, expression of *Ec*ODC was induced by adding 0.5 mM isopropyl thio-β-D-galactopyranoside. After 10 h of growth at 30 °C, corresponding to an absorbance at 600 nm of 3.5–3.8, the cells were harvested by centrifugation (2800 ***g***, 20 min, 4 °C). Approximately 20 g of cells were suspended in 40 mL 0.1 M sodium phosphate, pH 7.0, containing 0.1 mM ThDP/$MgSO_4$, 5% v/v glycerol, 1 mM phenylmethanesulfonyl fluoride, 1 mM dithiothreitol (DTT) and 1 mM EDTA, and disrupted using a French press (five passages at 1200 bar). The homogenate was clarified by centrifugation (70 000 ***g***, 30 min), and the supernatant was diluted to 40 mg protein$\cdot mL^{-1}$ using the same buffer. Nucleic acids were eliminated by streptomycin sulfate precipitation (0.1% w/v, 30 min agitation at 8 °C, and 25 min centrifugation at 70 000 ***g***). After two subsequent ammonium sulfate precipitations (15 g/100 mL each), the pellet was resuspended in 25 mM Tris/HCl, pH 7.5. The protein solution was dialysed twice for 5 h against 25 mM Tris/HCl, pH 7.5, 1 mM DTT, with or without 150 mM NaCl, and then further purified by anion-exchange chromatography using Q-Sepharose (GE Healthcare, Munich, Germany; column size, diameter 26 × length 100 mm). Elution was performed with a linear gradient of 500 mL of 100–400 mM NaCl in 25 mM Tris/HCl, pH 7.5. The *Ec*ODC-containing fractions, eluting at 150–300 mM NaCl, were pooled and precipitated by adding 32 g ammonium sulfate per 100 mL. After centrifugation (40 000 ***g***, 15 min), the pellet was resuspended in 50 mM MES/NaOH, pH 6.5, 0.2 M ammonium sulfate, applied on Superdex 200 (GE Healthcare; column size, diameter 26 × length 600 mm), and eluted at a flow rate of 0.5 mL$\cdot min^{-1}$ using the same buffer. Eluted fractions were analysed by SDS–PAGE. *Ec*ODC-containing fractions with > 95% homogeneity were pooled, flash-frozen in liquid nitrogen, and stored at −80 °C. The identity of the purified enzyme was confirmed using a combination of tryptic digestion and MALDI-TOF mass spectrometry.

Determination of protein concentration

The protein concentrations of samples containing absorbing ligands, such as ThDP, ADP, CoA or acetyl CoA, were determined by the Bradford assay [23] using BSA as the standard. Otherwise, the protein concentration was measured via UV absorbance using a calculated molar absorption coefficient of 44 600 $M^{-1}\cdot cm^{-1}$ at 280 nm for the *Ec*ODC monomer (http://www.expasy.ch/tools/protparam.html).

Synthesis of the substrate oxalyl CoA

Oxalyl CoA was synthesized by thiol ester interchange between thiocresol oxalate and CoA [24]. Thiocresol oxalate was synthesized as described previously [19]. The resulting product was purified by reverse-phase HPLC as described previously [17], but using a Lichrospher 100 column (Merck KgaA Darmstadt, Germany; diameter 4 × length 250 mm, particle size 12 μm) and a stepwise linear gradient at a flow rate of 1 $mL\cdot min^{-1}$.

Determination of the molar absorption coefficient of oxalyl CoA and formyl CoA

Synthesized and HPLC-purified oxalyl CoA was dissolved in 25 mM sodium phosphate, pH 6.5. The UV/Vis spectra for various dilutions were recorded using an Uvikon 941 spectrophotometer (Kontron Instruments, GmbH, Düsseldorf, Germany). After addition of 0.7 μM *Ec*ODC, the mixture was incubated for 15 min at 30 °C, resulting in complete conversion of oxalyl CoA to formyl CoA. UV/Vis spectra of the resulting solutions were recorded simultaneously (Fig. 6A). The decarboxylation of oxalyl CoA was followed by monitoring the $n \rightarrow \pi^*$ transition of the α carbonyl group of the substrate at 235 nm [7]. A molar absorption coefficient of 3300 $M^{-1}\cdot cm^{-1}$ was determined from the difference spectra and used for the calculation of catalytic activities.

Activity assay

Catalytic activities were determined using Jasco UV560 (Jasco Labor- u. Datentechnik GmbH, Groβ-Umstadt, Germany) or Uvikon 941 spectrophotometers in 25 mM sodium phosphate, pH 6.5 at 30 °C, with a final reaction volume of 300 μL. Over the typical time scale of several minutes, solvent-catalysed hydrolysis of the thioester is not detectable under these conditions (Fig. 6B). Prior to the measurements, the enzyme stock solution (1 $mg\cdot mL^{-1}$, 16.5 μM monomer) was saturated with the cofactors ThDP and $MgSO_4$ (both 250 μM) and incubated for 20 min at 30 °C. The reaction was started by addition of 15 μL enzyme solution to the reaction mixture. A dissociation constant of 17 μM was estimated for ThDP using fluorescence spectroscopy. The steady-state kinetic constants K_M and k_{cat} were determined by non-linear regression of the data for the corresponding plots of v against [S] according to the Michaelis–Menten equation.

Small-angle X-ray solution scattering

Data were collected using beamline X33 of the EMBL Hamburg Outstation (DORIS storage ring, Deutsches Elektronen Synchrotron, Hamburg, Germany). Measurements were performed at 16 °C with a camera length of 2.7 m using a MAR345 image plate detector and a new vacuum sample cell [25]. For s axis calibration ($s = 4\pi\sin\theta/\lambda$, where 2θ is the scattering angle and λ is 0.15 nm, the X-ray wavelength), collagen or tripalmitate was used. The scattering patterns were collected for 120 s. Primary image files were extracted during data collection for intensity normalization (transmitted flux, detector response, s axis scaling) using the data reduction program AUTOMAR [26]. *Ec*ODC samples were concentrated using centrifugal concentrators. If necessary, the buffer was exchanged simultaneously. The influence of protein concentration was studied for the range 0.7–23 mg *Ec*ODC·mL^{-1} in 0.1 M Bis/Tris, pH 6.4, 10 mM ThDP/$MgSO_4$, 5 mM DTT in the absence and presence of 5 mM coenzyme A. The effect of the activator ADP was investigated for the range 0–50 mM in the same buffer at a protein concentration of 5 $mg\cdot mL^{-1}$. The dependence of the oligomerization state of the enzyme on pH was measured from pH 5.6–9.5 in various buffers, each at 0.1 M ionic strength in the presence of 5 mM DTT in the absence or presence of 5 mM ThDP/$MgSO_4$ as well as 10 mM ADP at 5 mg enzyme·mL^{-1}. Immediately before and after the recording of protein scattering curves, the scattering pattern for a buffer containing all components except *Ec*ODC was measured. The scattering patterns of the buffer were merged and subtracted from the corresponding enzyme-containing patterns using the program PRIMUS-MAR [27]. The forward scattering intensity $I_{(0)}$ and the radius of gyration R_G were determined using the program GNOM [28]. The molecular masses of *Ec*ODC samples were calculated based on the ratio between the $I_{(0)}$ of *Ec*ODC and that of BSA (4 $mg\cdot mL^{-1}$) and the molecular mass of the latter (67 kDa). Theoretical scattering patterns were calculated from the crystal structure models using the program CRYSOL [16]; solution structure models were calculated from experimental scattering patterns using the program DAMMIN [29].

Crystallization

The purified *Ec*ODC was concentrated to 20 $mg\cdot mL^{-1}$, and the buffer was changed to 25 mM MES/NaOH, pH 6.5, 5 mM ThDP/$MgSO_4$ for the ThDP–*Ec*ODC complex. To obtain the complexes ThDP–ADP–*Ec*ODC or ThDP–acetyl CoA–*Ec*ODC, 10 mM ADP or 2 mM acetyl CoA were added. All *Ec*ODC complexes were crystallized by the

hanging drop vapour diffusion technique [30]. The drops contained equal volumes (2 μL) of reservoir solution and *Ec*ODC complex. The following reservoir solutions were applied: 100 mM MES/NaOH, pH 6.5 and 1.5 M ammonium sulfate for ThDP–*Ec*ODC, 100 mM MES/NaOH, pH 6.25 and 1.75 M ammonium sulfate for ThDP–ADP–*Ec*ODC, and 100 mM MES/NaOH, pH 6.0, 0.2 M sodium acetate and 5% w/v poly(ethylene glycol) 4000 for ThDP–acetyl CoA–*Ec*ODC. Typically, crystals appeared after 3 days of incubation at 8 °C.

Data collection

Crystals were incubated in cryosolutions containing 20% v/v ethylene glycol and 80% of the corresponding reservoir solution. Diffraction data were collected at 100 K using beamlines X12 and BW7A of the EMBL Hamburg Outstation (DORIS storage ring, Deutsches Elektronen Synchrotron, Hamburg, Germany) using detectors MARCCD-225 or MARCCD-165. The datasets were indexed, integrated and scaled using the programs DENZO and SCALEPACK [31]. Intensities were converted to structure factor amplitudes using the program TRUNCATE [32,33].

Structure determination and crystallographic refinement

Initial phases were obtained by using the molecular replacement method (program MOLREP [32]). The Expasy proteomics server (http://expasy.org/sprot/) [34] was used to generate a theoretical search model from the amino acid sequence of *Ec*ODC based on the structure of *Of*ODC (PDB ID 2c31). The asymmetric unit contains two monomers. Inspection of electron density maps, model building and refinement were performed using REFMAC5 [32] and COOT [35] until the free *R* factor and the crystallographic *R* factor could not be improved further. For calculation of the R_{free} values, 1% (ThDP–ADP–*Ec*ODC and ThDP–acetyl CoA–*Ec*ODC) and 5% (ThDP–*Ec*ODC) of reflections, respectively, were randomly chosen. The final models were validated using PROCHECK [35]. All crystal structure figures were prepared using PYMOL (http://www.pymol.org).

Acknowledgements

We gratefully acknowledge Dr Peter Konarev (EMBL Outstation Hamburg) for helpful discussions on interpretation of SAXS data using the program CRYSOL, Dr Johannes Steinreiber (Department for Organic Chemistry, University of Graz, Austria) for providing the plasmid used for expression of *Ec*ODC. Access to the EMBL beamlines X33, X12 and BW7A in Hasylab at the DORIS storage ring, Deutsches Elektronen Synchrotron, Hamburg, is acknowledged.

References

1 Hodgkinson A (1977) Oxalate content of foods and nutrition. In *Oxalic Acid in Biology and Medicine* (Hodgkinson A, ed), pp. 193–212. Academic Press, London.
2 Baetz AL & Allison MJ (1989) Purification and characterization of oxalyl-coenzyme A decarboxylase from *Oxalobacter formigenes*. *J Bacteriol* **171**, 2605–2608.
3 Berthold CL, Moussatche P, Richards NG & Lindqvist Y (2005) Structural basis for activation of the thiamin diphosphate-dependent enzyme oxalyl-CoA decarboxylase by adenosine diphosphate. *J Biol Chem* **280**, 41645–41654.
4 Berthold CL, Toyota CG, Moussatche P, Wood MD, Leeper F, Richards NG & Lindqvist Y (2007) Crystallographic snapshots of oxalyl-CoA decarboxylase give insights into catalysis by nonoxidative ThDP-dependent decarboxylases. *Structure* **15**, 853–861.
5 Muller YA, Lindqvist Y, Furey W, Schulz GE, Jordan F & Schneider G (1993) A thiamin diphosphate binding fold revealed by comparison of the crystal structures of transketolase, pyruvate oxidase and pyruvate decarboxylase. *Structure* **1**, 95–103.
6 Sahin N (2003) Oxalotrophic bacteria. *Res Microbiol* **154**, 399–407.
7 Quayle JR (1963) Carbon assimilation by *Pseudomonas oxalaticus* (Ox1). 7. Decarboxylation of oxalyl-coenzyme A to formyl-coenzyme A. *Biochem J* **89**, 492–503.
8 Gruez A, Roig-Zamboni V, Valencia C, Campanacci V & Cambillau C (2003) The crystal structure of the *Escherichia coli yfdW* gene product reveals a new fold of two interlaced rings identifying a wide family of CoA transferases. *J Biol Chem* **278**, 34582–34586.
9 Toyota CG, Berthold CL, Gruez A, Jónsson S, Lindqvist Y, Cambillau C & Richards NGJ (2008) Differential substrate specificity and kinetic behavior of *Escherichia coli* YfdW and *Oxalobacter formigenes* formyl coenzyme A transferase. *J Bacteriol* **190**, 2556–2564.
10 Hawkins CF, Borges A & Perham RN (1989) A common structural motif in thiamin pyrophosphate-binding enzymes. *FEBS Lett* **255**, 77–82.
11 Kaplun A, Binshtein E, Vyazmensky M, Steinmetz A, Barak Z, Chipman DM, Tittmann K & Shaanan B (2008) Glyoxylate carboligase lacks the canonical active site glutamate of thiamine-dependent enzymes. *Nat Chem Biol* **4**, 113–118.
12 Shukla A, Mylonas E, Di Cola E, Finet S, Timmins P, Narayanan T & Svergun DI (2008) Absence of equilibrium cluster phase in concentrated lysozyme solutions. *Proc Natl Acad Sci USA* **105**, 5075–5080.
13 Javid N, Vogtt K, Krywka C, Tolan M & Winter R (2007) Protein–protein interactions in complex cosolvent solutions. *Chemphyschem* **8**, 679–689.

14 Kutter S, Spinka M, Koch MHJ & König S (2007) The influence of protein concentration on oligomer structure and catalytic function of two pyruvate decarboxylases. *Protein J* **26**, 585–591.
15 Schütz A, Golbik R, Tittmann K, Svergun DI, Koch MHJ, Hübner G & König S (2003) Studies on structure–function relationships of indolepyruvate decarboxylase from *Enterobacter cloacae* – a key enzyme of the indole acetic acid pathway. *Eur J Biochem* **270**, 2322–2331.
16 Svergun D, Barberato C & Koch MHJ (1995) CRYSOL – a program to evaluate X-ray solution scattering of biological macromolecules from atomic coordinates. *J Appl Crystallogr* **28**, 768–773.
17 Jonsson S, Ricagno S, Lindqvist Y & Richards NG (2004) Kinetic and mechanistic characterization of the formyl-CoA transferase from *Oxalobacter formigenes*. *J Biol Chem* **279**, 36003–36012.
18 Bendazzoli C, Turroni S, Gotti R, Olmo S, Brigidi P & Cavrini V (2007) Determination of oxalyl-coenzyme A decarboxylase activity in *Oxalobacter formigenes* and *Lactobacillus acidophilus* by capillary electrophoresis. *J Chromatogr B Analyt Technol Biomed Life Sci* **854**, 350–356.
19 Stolle R (1914) Über Methylthionaphtenchinon. *Ber Dtsch Chem Ges* **47**, 1130–1132.
20 Sly W & Stadtman ER (1963) Formate metabolism: I. Formyl coenzyme A, an intermediate in the formate-dependent decomposition of acetyl-phosphate in *Clostridium kluyveri*. *J Biol Chem* **238**, 2632–2638.
21 Kern D, Kern G, Neef H, Tittmann K, Killenberg-Jabs M, Wikner C, Schneider G & Hübner G (1997) How thiamine diphosphate is activated in enzymes. *Science* **275**, 67–70.
22 Crosby J & Lienhard GE (1970) Mechanism of thiamine-catalyzed reactions. A kinetic analysis of the decarboxylation of pyruvate by 3,4-dimethylthiazolium ion in water and ethanol. *J Am Chem Soc* **92**, 5707–5716.
23 Bradford MM (1976) A rapid and sensitive method for the quantitation of microgram quantities of protein utilizing the principle of protein–dye binding. *Anal Biochem* **72**, 248–254.
24 Lipmann F & Tuttle C (1945) A specific micromethod for the determination of acyl phosphates. *J Biol Chem* **159**, 21–28.
25 Roessle MW, Klaering R, Ristau U, Robrahn B, Jahn B, Gehrmann T, Konarev P, Round A, Fiedler S, Hermes C *et al*. (2007) Upgrade of the small-angle X-ray scattering beamline X33 at the European Molecular Biology Laboratory, Hamburg. *J Appl Crystallogr* **40**, 190–194.
26 Petoukhov MV, Konarev PV, Kikhney AG & Svergun DI (2007) ATSAS2.1 – towards automated and web-supported small-angle scattering data analysis. *J Appl Crystallogr* **40**, 223–228.
27 Konarev PV, Volkov VV, Sokolova AV, Koch MHJ & Svergun DI (2003) PRIMUS: a Windows PC-based system for small angle scattering data analysis. *J Appl Crystallogr* **36**, 1277–1282.
28 Svergun DI (1992) Determination of the regularization parameter in indirect-transform methods using perceptual criteria. *J Appl Crystallogr* **25**, 495–503.
29 Svergun D (1999) Restoring low resolution structure of biological macromolecules from solution scattering using simulated annealing. *Biophys J* **76**, 2879–2886.
30 Hampel A, Labananskas M, Conners PG, Kirkegard L, RajBhandary UL, Sigler PB & Bock RM (1968) Single crystals of transfer RNA from formylmethionine and phenylalanine transfer RNA's. *Science* **162**, 1384–1387.
31 Otwinowski Z & Minor W (1997) Processing X-ray diffraction data collected in oscillation mode. *Methods Enzymol* **276**, 307–326.
32 Collaborative Computational Project (1994) The CCP4 suite: programs for protein crystallography. *Acta Crystallogr D Biol Crystallogr* **50**, 760–763.
33 French S & Wilson K (1978) Treatment of negative intensity observations. *Acta Crystallogr A* **34**, 517–525.
34 Schwede T, Kopp J, Guex N & Peitsch MC (2003) SWISS-MODEL: an automated protein homology-modeling server. *Nucleic Acids Res* **31**, 3381–3385.
35 Emsley P & Cowtan K (2004) Coot: model-building tools for molecular graphics. *Acta Crystallogr D Biol Crystallogr* **60**, 2126–2132.